RSC Advances

PAPER

View Article Online
View Journal | View Issue

Cite this: *RSC Adv.*, 2025, **15**, 22807

Comparative pharmacological studies on novel green-synthesized nano-zero-valent aluminum†

Fady Sayed Youssef,[a] Magdi E. A. Zaki,*[b] Nadeen Nasser,*[c] Sami A. Al-Hussain,[b] Gehad G. Mohamed[cd] and Omar A. Fouad[c]

This study aimed to synthesize nano-zero-valent aluminum (NZVAl) for its significant reactivity and reducing properties *via* a green synthesis method, which offers numerous advantages. Green-synthesized nano-zero-valent aluminum (GT-NZVAl) was synthesized at concentrations of 40 and 100 g L^{-1} and subsequently characterized using various techniques. The development of carbon and oxide outer layers in GT-NZVAl accounted for the material's exceptional stability, along with its economic and safety advantages. Subsequently, GT-NZVAl (40) and GT-NZVAl (100) were evaluated using the DPPH radical scavenging method to determine their antioxidant efficacy. HPLC and *in vitro* studies on their antioxidant activity (DPPH method), anti-inflammatory effects (membrane stabilization of COX-1 and COX-2), antimicrobial activity against *H. pylori* (MIC and MBC), and *in vivo* anti-inflammatory activity were conducted, which encompassed the assessment of various parameters (CRP, TNFα, and IL-6 levels). The findings of these analyses demonstrated that GT-NZVAl displayed notable anti-inflammatory efficacy, comparable to that of the standard indomethacin. The efficacy of the anti-inflammatory activity of GT-NZVAl at the two concentrations against COX-1 and COX-2 exhibited dose-dependent increase. *In vivo* anti-inflammatory study results indicated the potential anti-inflammatory effects of the newly developed nanoparticle formulation. GT-NZVAl (100) exhibited antioxidant activity comparable to that of GT-NZVAl (40) and the standard ascorbic acid. The percentage antioxidant activity increased in a dose-dependent manner across all the tested concentrations. The cytotoxicity of GT-NZVAl (40) and GT-NZVAl (100) on the normal human diploid cell line WI-38, as assessed *via* the MTT assay, yielded IC_{50} values of 302.96 μg ml^{-1} and 382.99 μg ml^{-1}, respectively.

Received 5th May 2025
Accepted 6th June 2025

DOI: 10.1039/d5ra03179f

rsc.li/rsc-advances

1. Introduction

Over the past few years, nanoparticles, whose size ranges from 1 to 100 nm, have garnered significant attention. Their nanosize endows them with outstanding characteristics compared with bulk particles, leading to their exploitation in several applications. Their substantial surface area explains their high surface-area-to-volume ratio, which is a crucial factor in determining their significant reactivity, chemical stability, adjustable porosity, and excellent mechanical properties.[1,2] In particular, nano-zero-valent metals (ZVMs) have generated considerable interests in the research domain owing to their reducing properties. The high effectiveness of nano-zero-valent metals (nZVMs) alters the ability of metals to undergo electron transfer and the stability of metals across various pH ranges.[3] Nano-zero-valent aluminum (NZVAl) is considered an effective zero-valent metal for use in various applications, such as water treatment, contaminant removal, and biological studies, owing to its ability to facilitate electron transfer.[4] Moreover, NZVAl is considered to have great potential as a reducing agent, adsorbent, and catalyst.[5] In the present study, a green synthesis method was used to fabricate nano-zero-valent aluminum (GT-NZVAl), which is a promising, eco-friendly, and cost-effective material with great potential in pollutant removal and biological applications.[6,7] In addition to the economic and safety benefits of GT-NZVAl, the remarkable stability of this material is observed due to the growth of carbon and oxide outer layers.

There are several factors influencing nanoparticle synthesis when using green synthesis methods. The most vital factor is the concentration of reducing agents, such as polyphenols in black tea. The importance of polyphenols can be summarized in their capping and reducing roles. Additionally, pH variations can play a role in the agglomeration of nanoparticles through excessive nucleation in an acidic medium or by producing

[a]*Pharmacology Department, Faculty of Veterinary Medicine, Cairo University, 12211 Giza, Egypt*
[b]*Department of Chemistry, Faculty of Science, Imam Mohammad Ibn Saud Islamic University (IMSIU), Riyadh 11623, Saudi Arabia. E-mail: mezaki@imamu.edu.eg*
[c]*Chemistry Department, Faculty of Science, Cairo University, 12613, Giza, Egypt. E-mail: nadeen@sci.cu.edu.eg*
[d]*Nanoscience Department, Basic and Applied Sciences Institute, Egypt-Japan University of Science and Technology, New Borg El Arab, Alexandria, 21934, Egypt*

† Electronic supplementary information (ESI) available. See DOI: https://doi.org/10.1039/d5ra03179f

unstable nanoparticles in a basic medium. At low pH, nanoparticle growth can manifest as agglomerated clusters; whereas at high pH, numerous pearl-like formations of nanoparticles may emerge alongside larger diameter nanoparticles.[8]

The idea behind the presented green synthesis procedure is that biologically active ingredients found in plant extracts can function as alternate reducing agents, and can react with metal salts to produce zero-valent metal nanoparticles. For instance, the stability of NZVI can also be increased using these organic components as dispersants and capping agents to successfully stop the nanoparticles from oxidizing and clumping together during the production process.[9] Wang *et al.* discovered that green-synthesized NZVI nanoparticles could maintain their activity in the air for two months, whereas the reactivity of chemically produced NZVI diminished by a factor of 2.1.[10] Various plant extracts encompass a diverse array of biomolecules and antioxidants, which influence the structural characteristics, dimensions, and reactivity of the synthesized metal nanoparticles.[11]

Machado *et al.* assessed the efficacy of 26 leaf extracts and discovered that optimal extractions could be achieved from leaves exhibiting a low level of moisture. This suggested that utilizing leaves that have naturally fallen from trees could offer benefits concerning both the process cost as well as the extract effectiveness. They also found that oak, pomegranate, and green tea extracts from the leaves exhibited greater antioxidant activity.[12]

Black tea, a widespread beverage derived from the leaves of the *Camellia sinensis* plant, has been savored for centuries and is noted for its distinctive flavor and potential health benefits. Over the past few years, increasing scientific studies have focused on investigating the bioactive components of black tea and their potential biomedical applications. In particular, black tea contains polyphenols, such as catechins and theaflavins, which possess potent antioxidant and anti-inflammatory properties. In addition to lowering inflammation and protecting cells from oxidative stress, these chemicals also help neutralize free radicals. Numerous studies have evidenced the power of black tea polyphenols to scavenge free radicals and inhibit inflammatory pathways, suggesting they may have potential applications in preventing chronic diseases.[13–15] Research suggests that black tea consumption may confer cardiovascular benefits. The polyphenols found in black tea have been found to enhance endothelial function, diminish blood pressure, and inhibit the oxidation of LDL cholesterol.[16]

Emerging evidence also suggests that black tea and its polyphenols may have cancer-preventive and anticancer properties, such as reducing cancer cell proliferation and increasing cell death. The aim of the present work was to investigate the synthesis of NZVAl by a green method using black tea extract and then to characterize it using various characterization techniques, including high-performance liquid chromatography (HPLC). Also, *in vitro* studies were performed, including assessing its antioxidant activity (DPPH method), anti-inflammatory (membrane stabilization of COX-1 and COX-2), and antimicrobial activity against *H. Pylori* (MIC and MBC). The *in vivo* anti-inflammatory activity was also assessed by testing different parameters (CRP, TNFα and IL-6 assay). It was hoped that the findings would shed more light on the effectiveness of NZVAl.

2. Materials and methods

Aluminum sulfate ($Al_2(SO_4)_3 \cdot 16H_2O$, 98.5% pure; Arabic Lab), ethyl alcohol (purity 95%, Sigma-Aldrich Chemie GmbH), acetone (95% pure; World Co.), and black tea were used as the main reagents. The *in vitro* study assessed the antioxidant activity (DPPH method), anti-inflammatory effects (membrane stabilization of COX-1 and COX-2), antimicrobial activity against *H. pylori* (minimum inhibitory concentration and minimum bactericidal concentration). The *in vivo* anti-inflammatory activity assessment involved testing various parameters, including C-reactive protein, tumor necrosis factor-alpha, and interleukin-6 assays.

2.1. Preparation of the black tea extract

Following acquisition from a local market, the extraction of black tea was performed by boiling approximately 40 and 100 g of black tea in 1 L of distilled water for 1 h at a temperature of 200 °C. The tea solutions were subsequently allowed to cool and were filtered with filter paper. The infiltrated dried tea was mixed with approximately 100 ml of a pure ethanol/acetone (50/50 ml) solution at ambient temperature for about 15 min, followed by filtration into the extracted tea solution to prevent aluminum oxidation. The tea solutions were subsequently extracted by re-filtering the mixture and were then preserved for future analysis.[6,17–19]

2.2. Synthesis of (GT-NZVAl)

The preparation of nano-zero-valent aluminum (GT-NZVAl-40) by a green synthesis method was executed utilizing black tea as a green source. In brief, around 6.843 g of $Al_2(SO_4)_3 \cdot 16H_2O$ was solubilized in a composite solution of ethanol and distilled water (approximately 100 ml of ethanol and 25 ml of distilled water). Next, 40 g L^{-1} extracted tea solution was added dropwise to the $Al_2(SO_4)_3 \cdot 16H_2O$ solution. Subsequently, the precipitate was dried at 150 °C after washing three times with 20 ml ethanol. Similarly, GT-NZVAl-100 was prepared by the same previous procedure but using 100 g L^{-1} extracted tea solution instead of 40 g L^{-1}.[3,7,17,20,21]

2.3. *In vitro* studies

2.3.1. Determination of the cytotoxicity of GT-NZVAl (40 and 100) on the human diploid cell line (WI-38) utilizing the MTT assay. A complete monolayer was established by incubating a 96-well tissue culture plate at a density of 1×10^5 cells per mL (100 μL per well) for approximately 24 h at 37 °C. The 96-well microplate's growth medium was removed after the confluent cell layer had formed, and the cellular monolayer was then washed twice with the washed medium. The test specimen was diluted by half in 2% serum-containing RPMI (maintenance medium). Three wells were allocated as the controls, and just supplied with the maintenance medium. A 0.1 ml sample of

every dilution was evaluated in each of the various wells. The plates were examined after being incubated at 37 °C. Any physical signs of toxicity in the cells were checked. An MTT assay was created (5 mg ml^{-1} in PBS) (Bio-Basic Canada Inc.). Next, 20 μL MTT solution was added to each well. The plate with the MTT solution mixed in the medium was then shaken for 5 min at 150 rpm to fully blend the two, and the medium was removed after 1–5 hours of incubation (at 37 °C with 5% CO_2). To remove any left-over residues, the plate was dried with a paper towel. Next, formazan (an MTT metabolite) was added to 200 μL of DMSO. To properly wet the formazan with the solvent, it was placed on the shaker for 5 min at 150 rpm. A direct correlation should exist between the optical density measured at 560 nm and the cell count following background subtraction at 620 nm.

2.3.2. Antioxidant activity of the aluminum formulations. The stable radical 2,2-diphenyl-1-picrylhydrazyl (DPPH) was employed to evaluate the free radical scavenging capacities of aluminum formulations in comparison to standard vitamin C, based on a method reported by Bhakya *et al.*[22]

2.3.3. Anti-inflammatory efficacy assessed through human red blood cell hemolysis and membrane stabilization assays. The process was carried out using the methodology reported by Anosike *et al.*[23]

2.3.4. Inhibition of COX-1 and COX-2. Analyses were conducted on all the synthesized compounds to determine whether they inhibit COX-1 and COX-2 (which were obtained under catalog no. 560131; Cayman Chemicals Inc. Ann Arbor, MI, USA). For the tested compounds, the selectivity index (SI) was calculated as IC_{50} (COX-1)/IC_{50} (COX-2). Additionally, celecoxib's IC_{50} values for COX-1 and COX-2 were determined.[24]

2.3.5. Antimicrobial efficacy against *H. Pylori*

2.3.5.1. Preparation of bacterial suspensions. The *H. pylori* strain was derived from Ain Shams Hospital as a clinical isolate. The strain was identified using the VITEK® 2 Compact system and confirmed by VITEK® MS in the 57357 Hospital, Egypt. An inoculum of the strain used in the susceptibility tests was prepared by transferring fresh colonies of the microorganisms. Newly formed microbial colonies were placed into tubes containing sterile physiological saline solution and by adjusting the turbidity to McFarland standard no. 2.[25] The turbidity resulted in a suspension of approximately 1.0×10^8 CFU ml^{-1} of *H. pylori*.

2.3.5.2. Assessment of the anti-H. pylori efficacy. The *in vitro* anti-*H. Pylori* activities were assessed using the good agar diffusion method.[26]

2.3.5.3. Minimal inhibitory concentration (MIC). The microdilution broth method, as described by the Clinical and Laboratory Standards Institute,[25] involves determining the tested sample's minimal inhibitory concentration (MIC) employing Mueller–Hinton broth enriched with lysed equine blood.

2.3.5.4. Minimum concentration required to kill bacteria (MBC). The minimum bactericidal concentration (MBC) was determined by subculturing 100 ml of microbial culture from each well demonstrating complete growth inhibition, along with the last positive well and the growth control, onto Mueller–Hinton agar plates supplemented with 10% sheep blood. The plates were subjected to microaerophilic conditions and incubated at 35 °C for 72 h. The MBC was determined as the lowest concentration of the sample that inhibited microbial growth. The MBC/MIC ratios were computed to ascertain the bactericidal or bacteriostatic effect of the tested sample. In our study, antibacterial agents were typically classified as bactericidal if the MBC/MIC ratio did not exceed four times the MIC.[27] Every experiment was conducted in triplicate. Representative data are presented.

2.3.6. *In vivo* anti-inflammatory effect of GT-NZVAl (40 and 100)

2.3.6.1. Handling of the experimental animals. The guidelines for experimental research ethics established by the Research Ethics Committee of Cairo University's Faculty of Veterinary Medicine in Giza, Egypt, were observed when handling animals (VET CU 08072023665). The animals were maintained in the Animal House at Cairo University's Faculty of Veterinary Medicine. They were kept in tidy plastic cages with metal covers and wood flakes covering the ground. There was a 12 h light/dark cycle. The animals underwent a seven day passive preparatory phase to acclimate to their new surroundings and to check on their physical health.[27]

2.3.6.2. Anti-inflammatory effect tests. Thirty rats of both sexes weighing 150–200 g in body weight were used, as designated by Domenjoz *et al.*[28] All the rats were injected subcutaneously with 0.1 ml of 6% formalin solution in normal saline to induce inflammation in the right paw. Each group of five rats was separated into four equal groups. As a control group, the rats from the first group were only induced with inflammation. A standard dose of indomethacin (10 mg kg^{-1} body weight) was administered orally to those in the second group. GT-NZVAl-40 and GT-NZVAl-100 were administered orally to the rats in the third and fourth groups. To induce swelling, 0.1 ml of a 6% formalin solution in normal saline was subcutaneously injected into the right paw of each rat 30 min following the administration of the drug or test compound. After 1, 2, 3, 4, 5, and 6 h of administration, the thickness of each rat paw was assessed with Vernier calipers in mm. We then collected blood samples from each group's rats and tested them for inflammatory markers (CRP, TNF, IL-6).

All the animal procedures were performed and approved in accordance with the Guidelines for Care and Use of Committee (IACUC) of Vet Cairo University. The Research Ethics Committee of Cairo University's Faculty of Veterinary Medicine in Giza, Egypt, established guidelines for experimental research ethics were observed when handling animals (VET CU 08072023665). The Institutional Animal Care and Use Committee (IACUC) approved the referenced Animal Use Protocol (AUP). The human diploid cell line WI-38 and the human red blood cells used in this study were purchased from Prof. Sayed at the Faculty of Science, Al-Azhar University, and handled according to the supplier's guidelines.

2.4. Reactive protein assay procedures

These were performed and evaluated according to the method described by Kilpatrick and Bunk.[29]

2.5. TNFα and IL-6 assay procedures

These were performed and assessed according to the method reported by Afshari *et al.*[30]

2.6. Analysis of the statistical data

The results were presented as mean ± SEM. The data were analyzed using statistical software SPSS version 20.0. Duncan's Multiple Range test was used to distinguish between significant means at $P < 0.05$.

2.7. Instruments

The phase composition of the sintered samples and synthesized nanoparticles was examined using a Bruker D8 Discover X-ray diffractometer that utilized Cu K radiation that was Ni-filtered with $\lambda = 1.5406$ Å. In the gas-adsorption experiments, nitrogen (N_2) was used as the adsorptive gas to determine the BET surface area at 77 K. The materials were evacuated under high vacuum for 4 to 12 h before the adsorption test. The assessment was carried out using a Nova Touch LX2 analyzer, and the computation was based on Brunauer–Emmett–Teller (BET) theory. Scanning electron microscopy (SEM; Philips XL30) was used to analyze the microstructure and pore-size distribution of the samples. The SEM instrument was operated at an accelerating voltage of 30 kV, a magnification of up to 400 000, and a resolution of 3.5 nm. A thin layer gold coating was applied to the samples before testing. Using transmission electron microscopy (TEM; JEOL JEM-2100, Tokyo, Japan), the size and shape of the synthetic nanoparticles were examined. HPLC analysis was carried out with the aid of an Agilent 1260 series detector, with a Zorbax Eclipse Plus C8 column (4.6 mm × 250 mm i.d., 5 μm) used for the separation, at a flow rate of 0.9 ml min^{-1}, with water used as mobile phase A and 0.05% trifluoroacetic acid in acetonitrile as mobile phase B. The linear gradient programming that was used for the mobile phase: starting at 0 minutes, followed by 0 to 1 minute, then 1 to 11 minutes, then 18 to 22 minutes, and finally, 22 to 24 minutes (82% A). The 280 nm wavelength was used to record the multi-wavelength detector. A volume of 5 microlitres was injected into every one of the sample solutions. A constant temperature of 40 °C was used for the column.

3. Results and discussion

3.1. Mechanism of action of black tea as a reducing agent

Black tea was used as a reducing agent for synthesizing diverse morphologies of zero-valent metal nanoparticles owing to its abundant polyphenols and other organic compounds. Research has indicated that approximately 4000 species of polyphenols exist, of which one-third comprise polyphenols that facilitate the diminution of salt precursors to nanoparticles. Polyphenols are composed of flavonoids and catechins. The catechins, including epigallocatechin gallate (EGCG), epigallocatechin (EGC), epicatechin gallate (ECG), and epicatechin (EC), are noteworthy compounds. The concentration of catechins present in tea leaves is contingent upon their maturation stage. Typically, the concentration is greater in leaves utilized for black tea production compared to those employed in green tea production.[31] Epigallocatechin gallate (EGCG) is one of the most active components in the reduction process, possessing a standard potential of 0.57 V. This characteristic facilitates the reduction of Al^{+3} to Al^0 ($Al^{+3} + 3e^- \rightarrow Al^0$), given that Al^{+3} has a standard potential of −1.676 V.[32] In the presence of polyphenol radicals,

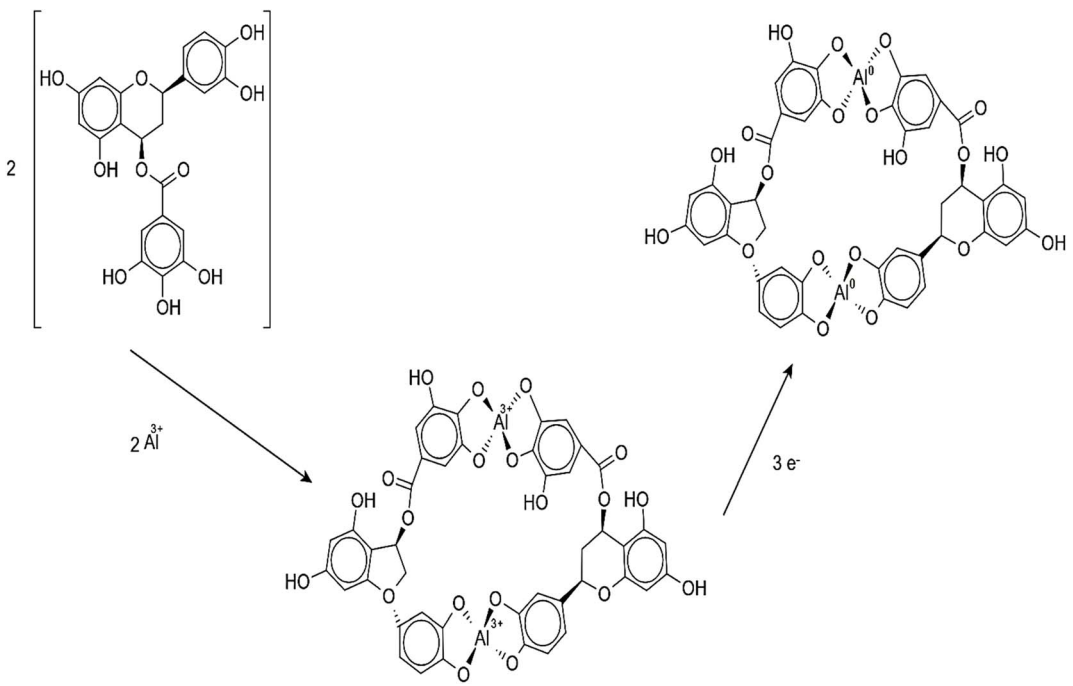

Fig. 1 Potential chelation reactions occurring between EGCG and Al^{3+} ions.

free Al^{3+} can be reduced to Al^0 by forming chelates, as shown in Fig. 1.[33] The reduction mechanism occurs in two distinct phases. First, when the Al^{+3} is added, the –OH bond is broken, establishing a complex that results in the formation of a partial bond with a metal ion. The reduction of metal ions into zero-valent aluminum nanoparticles is thus made possible by the partial bond breaking and electron transference.[32]

A small fraction of Al^{+3} may undergo oxidation by dissolved oxygen in the solution; however, the concurrent production of Al^0 could impede the oxidation of Al^{+3}.[33] So, tea polyphenol serves dual functions: it acts as a reductant for the synthesis of low biotoxicity zero-valent Al nanoparticles and functions as a capping agent to improve their stability and oxidation resistance.[33]

3.2. FTIR study

As illustrated in Fig. 2, the FTIR spectra of the synthesized GT-NZVAl (40 and 100) compounds in the range of 400–4000 cm^{-1} showed the functional groups present in the tea extract solutions. Nearly, the same peaks were present in the synthesized GT-NZVAl 40 and 100, as shown in Fig. 2. Significant broad peaks were observed in the range of 3000–3400 cm^{-1}, which were attributed to the presence of O–H stretching vibrations brought about by the extracted tea's phenolic group content. Also, the peak observed at 1710 cm^{-1} corresponded to the carbonyl group, which is part of the EGCG structure shown in Fig. 1. The polyphenol aromatic ring C=C stretching vibration was responsible for the peak at 1635 cm^{-1}, while the C–O–C symmetric stretching absorption was responsible for the peak at 1020 cm^{-1}. Additionally, prominent peaks were observed between 800 and 400 cm^{-1}, which were related to alkane aromatic compounds.[34,35] Subsequently, the presence of polyphenolic and aromatic groups was confirmed and they help enhance the stability of nanoparticles.[34,35] This data also matched with those for previously reported nanoparticles synthesized from tea extracts. Gottimukkala *et al.*[32] reported that iron nanoparticles manufactured using tea extract exhibited a broad O–H stretch at 3419 cm^{-1}, C=C at 1635 cm^{-1}, C–H at 2923 cm^{-1}, and C–O–C at 1020 cm^{-1}, respectively, in FTIR analysis. Also, C. Xiao *et al.* indicated that iron nanoparticles synthesized using tea extract displayed a large O–H stretch at 3388 cm^{-1}, C=C band at 1636 cm^{-1}, C–O–C at 1039 cm^{-1} and C–H at 2852 cm^{-1} in FTIR analysis.[33] Thus the previously reported results closely align with the extracted spectral features and validated our synthesis for preparing zero-valent aluminum *via* a green method.

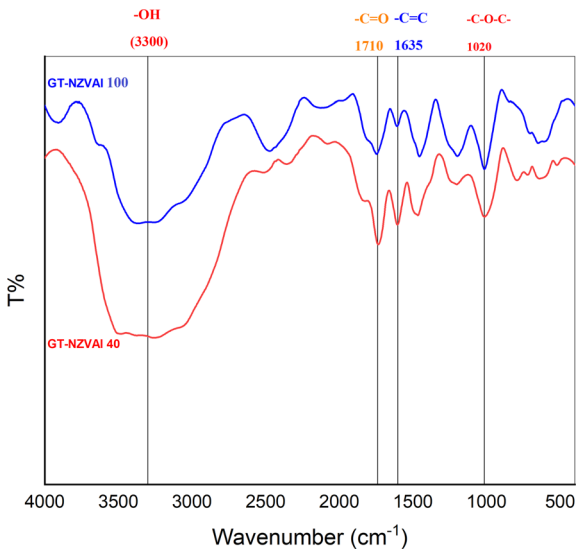

Fig. 2 FTIR spectra of the synthesized GT-NZVAl 40 and GT-NZVAl 100.

3.3. XRD patterns of the synthesized GT-NZVAl (40 and 100)

The XRD patterns of the synthesized GT-NZVAl (40 and 100) (Fig. 3) showed diffraction peaks for face-centered cubic aluminum at 38.5° (main diffraction peak), 44.7°, 65.1°, and 78.2°, attributed to the (1 1 1), (2 0 0), (2 2 0) and (3 1 1) planes, respectively.[36] In addition, the XRD patterns showed diffraction peaks at 31.2°, 40.2°, and 55.1°, which were ascribed to the (101), (232), and (110) planes of Al_4C_3,[37] as well as other peaks indicative of organic materials from green tea extract.[38] Furthermore, there is a chance that a tiny amount of aluminum metal was moderately oxidized through the washing and preparation procedures.[39] Hence, the synthesized aluminum particles consisted of an Al^0 aluminum core surrounded by an oxide and carbide shell, which serves as an inert barrier to shield the aluminum from additional oxidation.[40] It was also noted from the XRD data that the ratio of Al_4C_3 and Al_2O_3 compared to Al^0 was very low, indicating that Al^0 was the main phase in GT-NZVAl (40 and 100). Furthermore, it was observed that the crystallinity of GT-NZVAl decreased when the amount of tea extract (40 to 100 g L^{-1}) was increased. As the concentration of the extract increased, the organic coating layer derived from the green tea thickened and its crystallinity diminished, thereby affecting the XRD results.[34]

3.4. SEM of GT-NZVAl

SEM images of the GT-NZVAl (40 and 100) nanopowders are displayed in Fig. 4. The GT-NZVAl (40 and 100) powders exhibited an asymmetrical surface with a large number of irregular and noncircular pores. Additionally, SEM revealed that the NZVAl nanoparticles coated by the organic coating from the tea had a high degree of stability and formed irregular, spherical particles, which allows good dispersal of the nanoparticles.[34] Fig. 4 shows SEM images of the particles and the Gaussian fitting of the particle-size distribution, as well as histograms of the particle-size distribution, obtained using ImageJ (1.53e). The synthesized NZVAl had particle sizes ranging from 11.1 to 64.752 nm, with a mean size of 26.5 nm for NZVAl (40) and 28.9 nm for NZVAl (100). This variation in particle size was due to the presence of the natural organic coatings, which could improve the stability of the nanoparticles, facilitating their dispersion at first. After that, particles started rearranging, leading to their agglomeration.

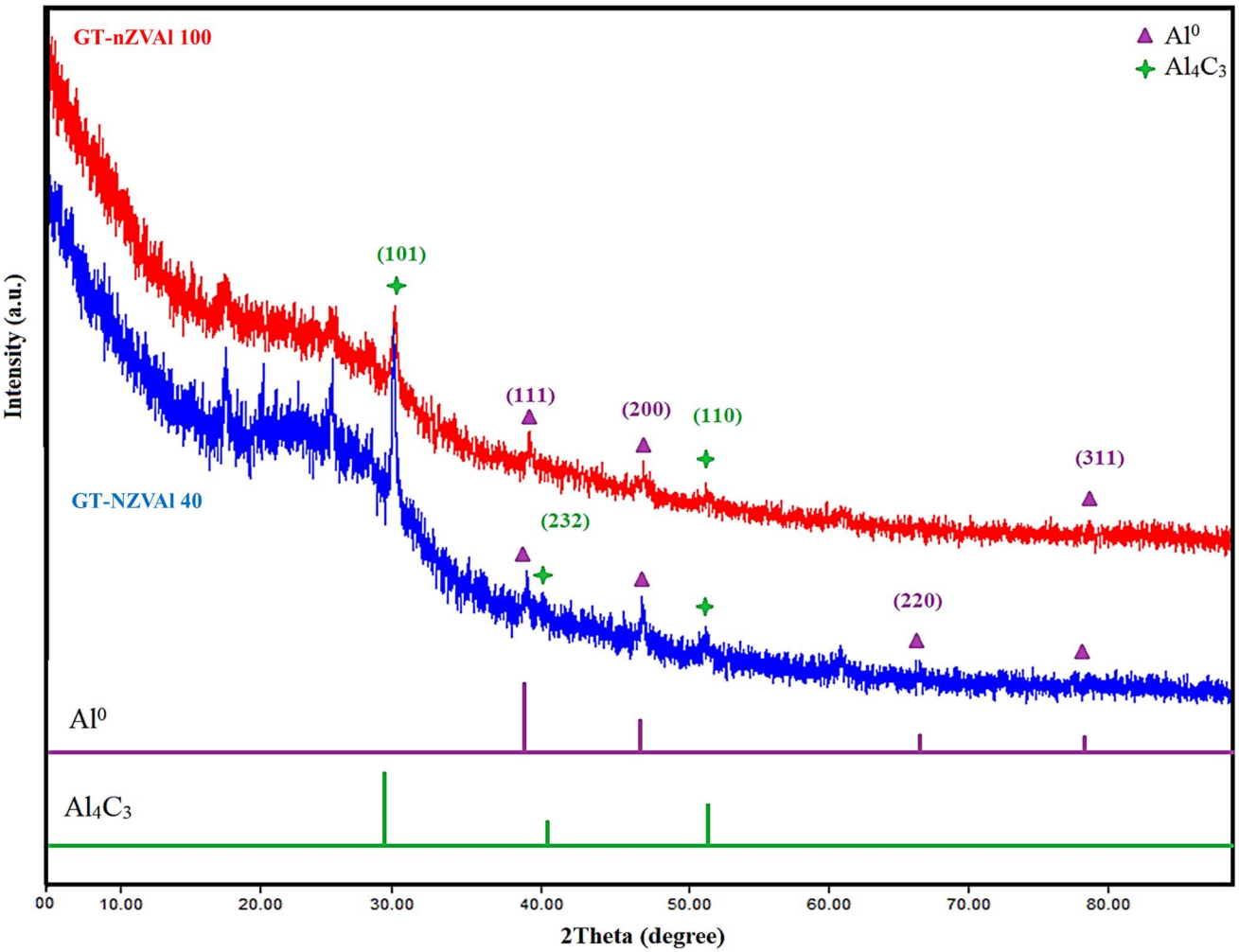

Fig. 3 XRD patterns of the synthesized GT-NZVAl (40 and 100).

3.5. TEM study of GT-NZVAl (40 and 100)

The TEM images, along with the Gaussian fitting of the particle-size distribution GT-NZVAl (40 and 100), as well as histograms of the particle-size distribution (Fig. 5A–D), revealed the presence of spherical nanoparticles of varying sizes, from 19.90 to 24.7 nm, with irregular and spherical particles. The average particle sizes were 8.9 nm for GT-NZVAl (40) and 9.1 nm for GT-NZVAl (100), indicating that GT-NZVAl had a smaller and more uniform size.

3.6. BET analysis

According to nitrogen adsorption–desorption theory, the surface areas, total pore volumes, and average pore sizes of GT-NZVAl (40) and GT-NZVAl (100) were 53.6183 $m^2\ g^{-1}$, 0.244192 $cm^3\ g^{-1}$, and 9.10852 nm and 61.7423 $m^2\ g^{-1}$, 0.149974 $cm^3\ g^{-1}$, and 4.85807 nm, respectively. So, they showed significant surface areas and mesoporous structures. As proved by the BET results, when increasing the concentration of black tea, the surface area increased. This was attributed to the high existence of polyphenols, which act as reducing and capping agents for metal ions, leading to a substantial decrease in the aggregation of the nanoparticles.[41] On the other hand, the pore volume decreased with high concentrations of black tea. This may be due to the interference of fine tea particles in the pores of the nanoparticles.

3.7. *In vitro* studies

3.7.1. Cytotoxicity. The cytotoxicity of GT-NZVAl (40) and GT-NZVAl (100) on the normal human diploid cell line (WI-38) was assessed using the MTT protocol. The results were represented as $IC_{50} \pm$ SD values, and were found to be 302.96 ± 4.47 and 382.99 ± 12.65 μg ml^{-1} for GT-NZVAl (40) and GT-NZVAl (100), respectively (Fig. 6–12). Statistical analysis was conducted using one-way ANOVA, followed by Duncan's multiple comparison tests, with significance set at $P < 0.05$.

3.7.2. Antioxidant activity of GT-NZVAl. The DPPH radical scavenging method was utilized to test the antioxidant activity of GT-NZVAl (40 and 100) at various concentrations (100, 50, 25, 12.5, 6.25, 3.12, 1.56 μg ml^{-1}). GT-NZVAl (100) showed antioxidant activity that was comparable to that of GT-NZVAl (40) Trolox. The percentage antioxidant activity escalated in a dose-dependent fashion across all the tested concentrations. Both

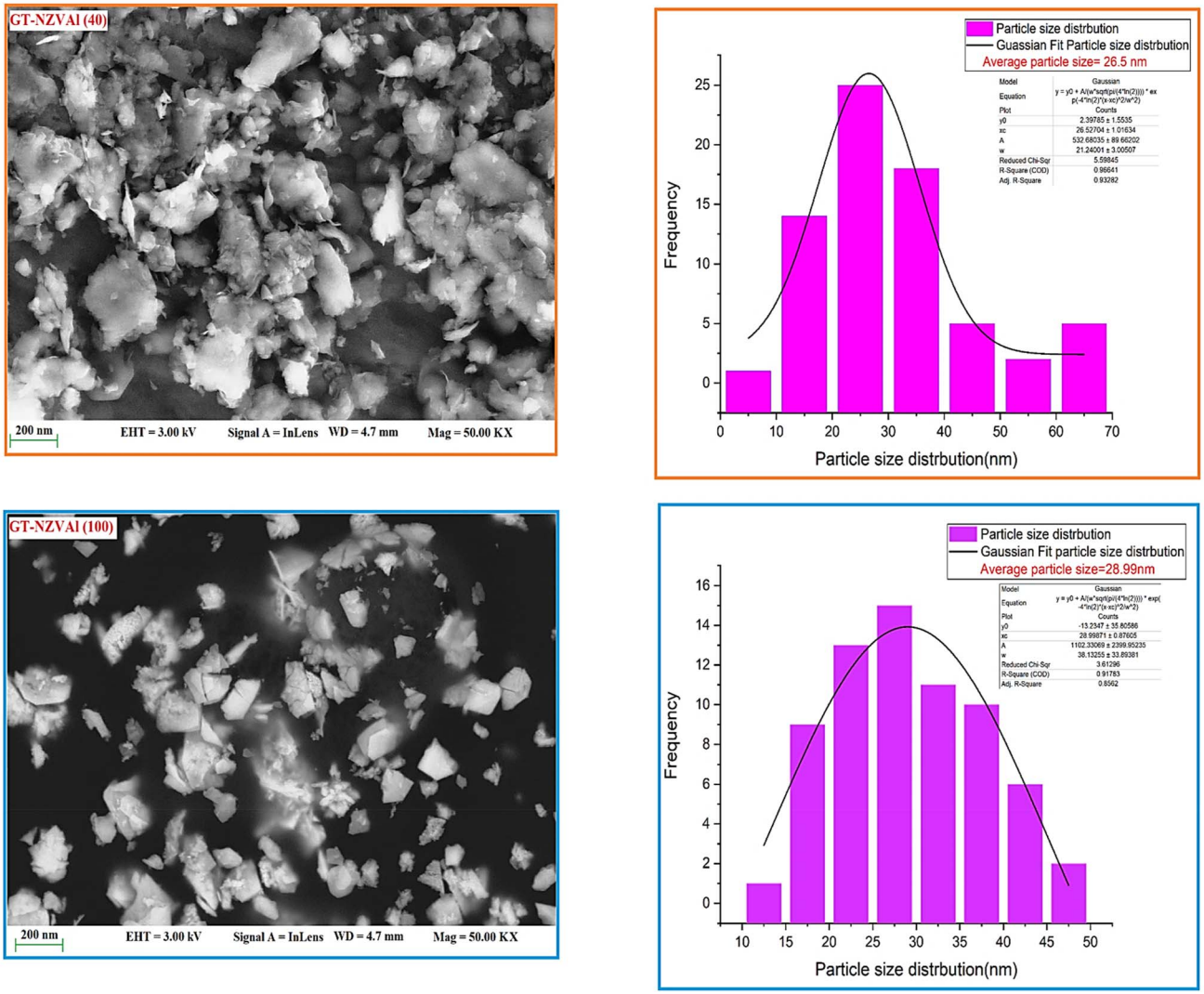

Fig. 4 SEM images of GT-NZVAl (40) and GT-NZVAl (100), and their particle-size distributions.

samples exhibited significant DPPH radical scavenging capabilities, as illustrated in Table 1.

3.7.3. Anti-inflammatory efficacy utilizing human red blood cell hemolysis and membrane stabilization assays. Using a method to stabilize the membranes of human red blood cells, the anti-inflammatory activity of GT-NZVAl was assessed *in vitro*. One way to measure a substance's ability to stabilize human red blood cell (RBC) membranes is to look at how well it prevents the destruction of RBC membranes. This approach is constructed on the idea that definite compounds can stabilize red blood cell membranes, making them less susceptible to stress-induced breakdown. The extent of hemolysis, outlined as the breakdown of red blood cells (RBCs), can be subsequently quantified employing a spectrophotometer or alternative techniques, such as assessing hemoglobin release. The degree of stabilization of the RBC membrane can be measured by assessing the percentage of hemolysis inhibition. This method is commonly employed to assess the potential detrimental impacts of drugs and chemicals on red blood cell membranes and was also utilized herein. The results indicated that GT-NZVAl demonstrated significant anti-inflammatory action comparable to that of the standard (indomethacin). Indomethacin demonstrated hemolytic inhibition percentages of 94.2 ± 0.01%, 90.5 ± 0.02%, 82.2 ± 0.01%, 73.1 ± 0.02%, 60.3 ± 0.01%, and 51.3 ± 0.01%, compared to 98.3 ± 0.01%, 94.6 ± 0.03%, 90.2 ± 0.02%, 88.3 ± 0.01%, 76.4 ± 0.05%, and 65.1 ± 0.03% for GT-NZVAl (100), respectively, as illustrated in Table 2.

3.7.4. Inhibitory effects on COX-1 and COX-2. The data presented in Table 3 show the inhibitory effects (inhibition percentages) of different compounds (celecoxib, GT-NZVAl (40), and GT-NZVAl (100)) across varying concentrations of COX-1 and COX-2. Each compound exhibited a dose-dependent inhibition pattern. Celecoxib demonstrated lower IC_{50} values (0.50 ± 0.15 and 0.09 ± 0.001 μm), indicating a relatively higher concentration required for 50% inhibition compared to GT-NZVAl (40) (2.60 ± 0.08 and 0.25 ± 0.01 μm) and GT-NZVAl (100) (1.40 ± 0.07 and 0.16 ± 0.01 μm) for COX-I and COX-2, respectively. Celecoxib showed the lowest IC_{50} value,

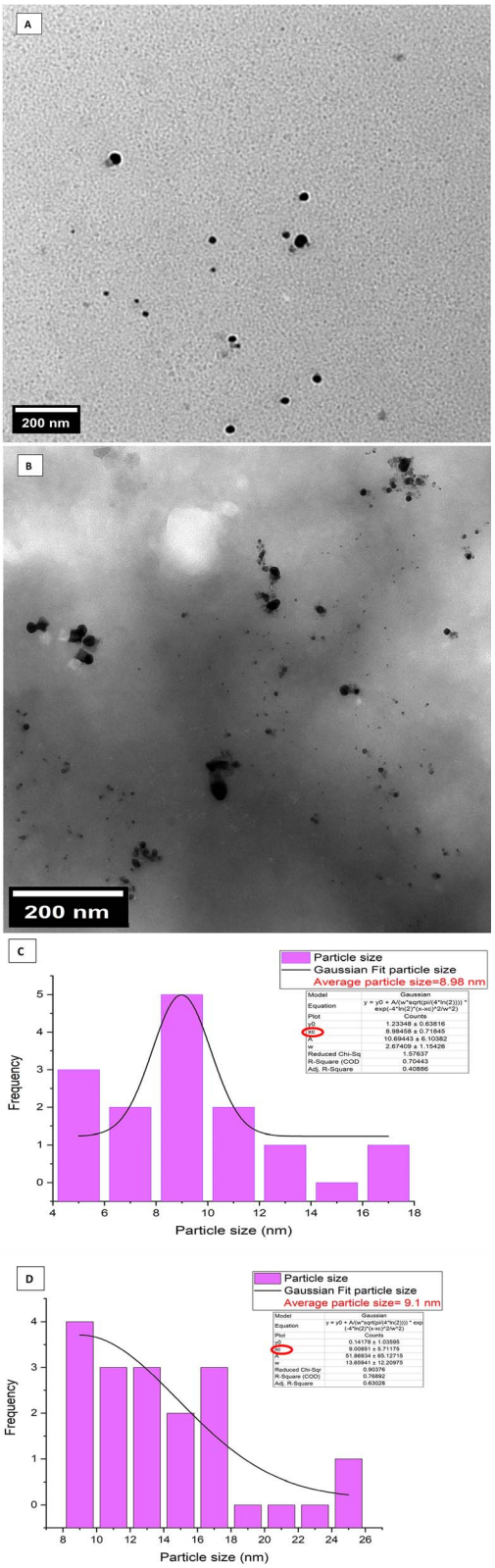

Fig. 5 HR-TEM images (A) and (B) of the prepared GT-NZVAl (40 and 100) and their particle-size distributions (C and D).

suggesting it is the most potent at inhibiting the target enzyme or process at lower concentrations. GT-NZVAl (40) fell between celecoxib and GT-NZVAl (100) in terms of potency, with an IC_{50} value of 7.5 μm. The results suggested that celecoxib was the most potent among the tested compounds, followed by GT-NZVAl (100) and then GT-NZVAl (40). These findings provide valuable insights into the comparative efficacy of these compounds in inhibiting a target enzyme or process, which is crucial for potential therapeutic applications or further research in pharmacology and medicine.

The selectivity index (SI) values were obtained and are also presented in Table 3. Celecoxib, a well-known COX-2 selective inhibitor, had an SI of 5.56, indicating that it inhibited COX-2 over COX-1 by approximately 5.56 times. This aligns with celecoxib's known pharmacological profile as a COX-2 selective non-steroidal anti-inflammatory drug (NSAID), reducing inflammation while minimizing COX-1-related gastric side effects. On the other hand, the GT-NZVAl (100) (SI = 8.75) compound had the highest selectivity index, indicating it was the most COX-2 selective among the tested drugs. It inhibited COX-2 over COX-1 by a factor of 10.4, meaning it could be a potential candidate as a COX-2-selective drug with fewer COX-1-related side effects. This makes it potentially superior to celecoxib in terms of selectivity. GT-NZVAl (40) (SI = 2.08) also demonstrated strong COX-2 selectivity. It was less selective than GT-NZVAl (40) but more selective than celecoxib. This suggests that increasing the concentration from 40 to 100 μM did not proportionally enhance the selectivity, indicating a possible saturation effect.

3.7.5. Assessment of the anti-*H. pylori* efficacy. An anti-*H. pylori* study was performed in triplicates as shown in (Fig. 13–15). GT-NZVAl (40) demonstrated a lower zone of inhibition value (25 ± 0.19 mm), indicating that a relatively higher concentration was required for the inhibition compared to GT-NZVAl (100) (31.7 ± 0.001 mm), thereby suggesting it was more potent at inhibiting *H. pylori* compared to GT-NZVAl (40), as shown in Fig. 13, 14A and B. These outcomes offer vital perspectives into the comparative efficacy of these compounds in inhibiting *H. pylori* in a dose-dependent manner. The minimum inhibitory concentration (MIC) and minimum bactericidal concentration (MBC) values are presented in Fig. 15. The MIC and MBC values indicate the effectiveness of tested drugs at inhibiting and killing bacteria. GT-NZVAl (40) had an MIC of 62.5 μg ml^{-1}, and MBC of 62.5 μg ml^{-1}, while its MBC/MIC index was equal to 1; since the MBC/MIC index equals 1, this suggests that GT-NZVAl (40) has a bactericidal effect (kills bacteria rather than just inhibiting growth). A ratio close to 1 generally means a drug efficiently kills bacteria at a concentration similar to its inhibitory concentration. On the other hand, GT-NZVAl (100) had an MIC of 31.25 μg ml^{-1} and MBC of 52.5 μg ml^{-1}, and an MBC/MIC index equal to 0.5. An MBC/MIC index equal to 0.5 indicates a strong bactericidal effect. This means GT-NZVAl (100) was even more potent than GT-NZVAl (40), as it required a lower MIC and a lower MBC while still being bactericidal. On the other hand, amoxicillin (the reference drug) had an MIC of 54.5 μg ml^{-1} and MBC of 57.6 μg ml^{-1}, and an MBC/MIC index equal to 0.95, suggesting a bactericidal effect similar to GT-NZVAl (40). However, GT-NZVAl (100) showed a lower MIC than amoxicillin, meaning it was more potent at inhibiting bacterial growth. GT-NZVAl (100) was the most potent drug in this study, as it had the lowest MIC

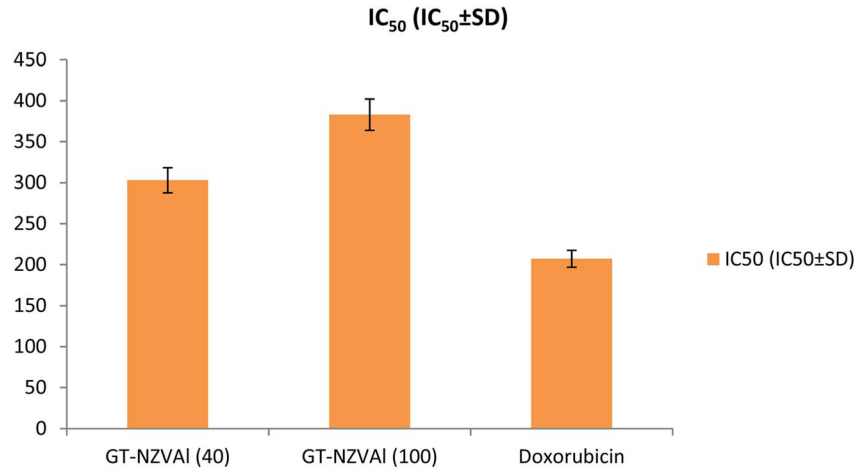

Fig. 6 Cytotoxicity assessments of doxorubicin, GT-NZVAl (40) and GT-NZVAl (100) on WI-38 cells utilizing the MTT assay.

(31.25 μg ml^{-1}) and an MBC/MIC index indicating strong bactericidal activity. GT-NZVAl (40) and amoxicillin both had similar effects, but GT-NZVAl (40) required a higher concentration (MIC = 62.5 μg ml^{-1}) to inhibit bacterial growth. The lower MIC of GT-NZVAl (100) suggests it could be an effective alternative to amoxicillin, with possibly better efficacy at lower doses.

3.7.6. *In vivo* anti-inflammatory effects

3.7.6.1. Anti-inflammatory effect on the thickness of rat paw edema. The consequences confirmed that GT-NZVAl (40) revealed potent anti-inflammatory activity comparable to that of the standard drugs indomethacin, meloxicam, and ketoprofen. GT-NZVAl (100) showed superior performance and was more promising for all groups due to its inhibition of paw edema thickness. The acquired data are illustrated in Fig. 16.

3.7.6.2. Anti-inflammatory effect considering inflammatory markers (CRP (C-reactive protein), TNFα and IL-6). The results indicated that GT-NZVAl (40) demonstrated significant anti-inflammatory activity comparable to that of the standard indomethacin. GT-NZVAl (100) showed superior performance and was more promising for all groups due to its inhibition of the inflammatory markers (CRP, TNFα, and IL-6) (Fig. 17).

4. Discussion

Black tea is recognized for its antioxidant properties, primarily due to its elevated levels of polyphenols, especially catechins and theaflavins. These antioxidants safeguard the body's cells from damage inflicted by detrimental free radicals. Below are several references that detail the antioxidant properties of black tea. Cabrera *et al.*[13] provided an overview of the antioxidant properties of tea, including black tea, and discussed the potential health advantages associated with its intake. McKay *et al.*[14] reviewed the current scientific evidence on the health benefits of tea, including its antioxidant activity, and discussed its prospective function in the prevention of chronic illnesses.

Arent *et al.*[42] surveyed the antioxidant impacts of black tea extract enriched with theaflavins in healthy smokers, demonstrating a reduction in oxidative stress markers and an augmentation of the antioxidant defense mechanism. Zhao (2019)[43] evaluated the total antioxidant capacity of various teas,

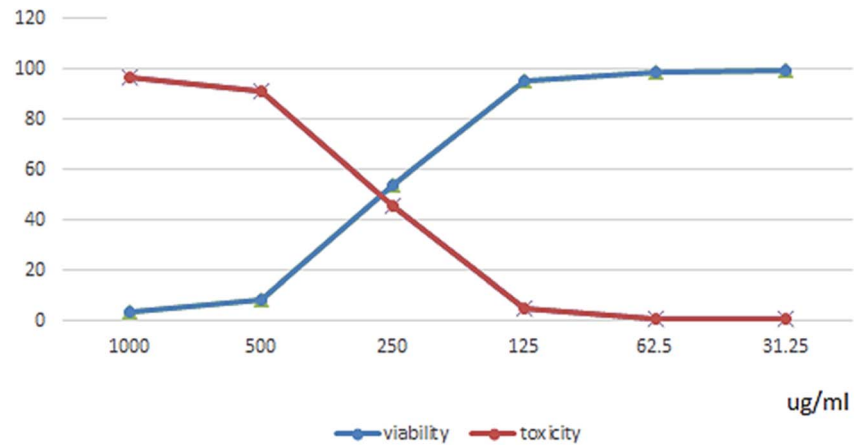

Fig. 7 Effect of GT-NZVAl (40) on WI-38 cells at different concentrations.

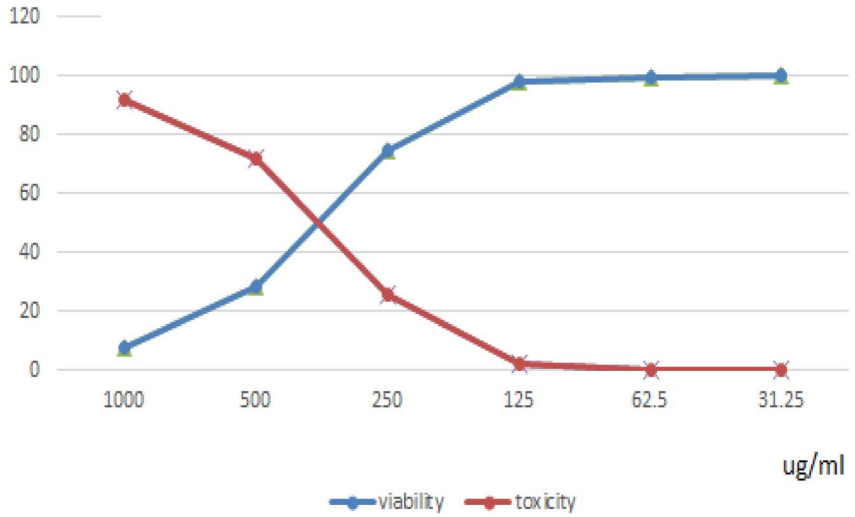

Fig. 8 Effect of GT-NZVAl (100) on WI-38 cells at different concentrations.

including black tea, utilizing the ferric reducing/antioxidant powder (FRAP) assay, providing quantitative data on the antioxidant action of black tea compared to other tea varieties. Black tea has been widely studied for its potential anti-inflammatory activity, which might be credited to its bioactive compounds, such as polyphenols and flavonoids. These compounds have demonstrated anti-inflammatory properties in various *in vitro* and *in vivo* investigations.

Here are a few references that provide information on the anti-inflammatory activities of black tea. Kuriyama *et al.*[44] probed the association between green tea utilization (which also includes black tea) and mortality attributable to cardiovascular disease, cancer, and all causes. Their findings suggested that regular tea consumption is associated with reduced mortality from these causes, which may be accredited, in part, to the anti-inflammatory effects of tea. Meng *et al.*[45] discussed the potential of natural products, including tea, in the avoidance and management of chemically induced hepatic injuries, highlighting the anti-inflammatory properties of tea and its potential role in protecting against liver inflammation. Reygaert *et al.*[46] studied the anti-inflammatory activity of black tea theaflavins and the mechanisms by which theaflavins apply their anti-inflammatory impacts. They provided an overview of *in vitro* and *in vivo* studies supporting the anti-inflammatory properties of black tea theaflavins. Shen *et al.*[47] discussed the role of dietary phytochemicals, including tea polyphenols, in bone protection, and highlighted the anti-inflammatory impacts of tea polyphenols and their potential in preventing inflammation-related bone loss. Some studies have also suggested the potential of tea polyphenols to modulate inflammatory responses.

Here are a few references that discuss the anti-inflammatory activity of zero-valent metallic compounds. Yen *et al.*[48] investigated the cytotoxicity and immunological response of gold and

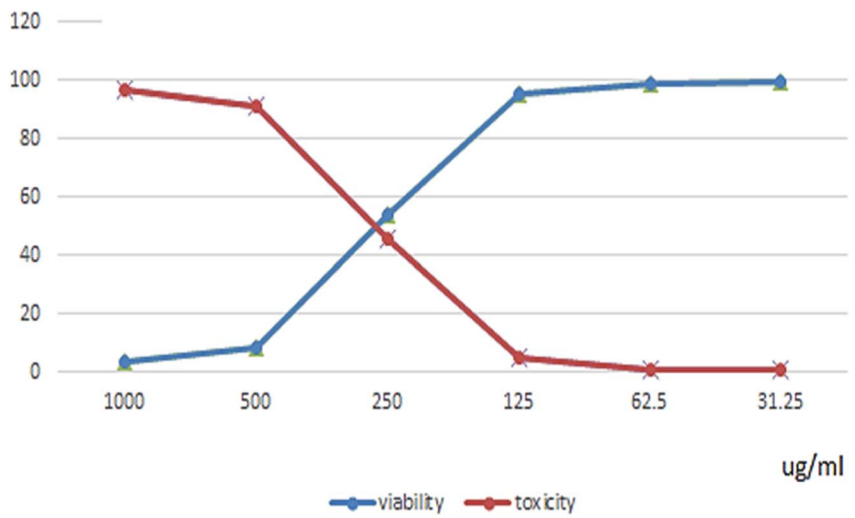

Fig. 9 Effect of standard doxorubicin on WI-38 cells at different concentrations.

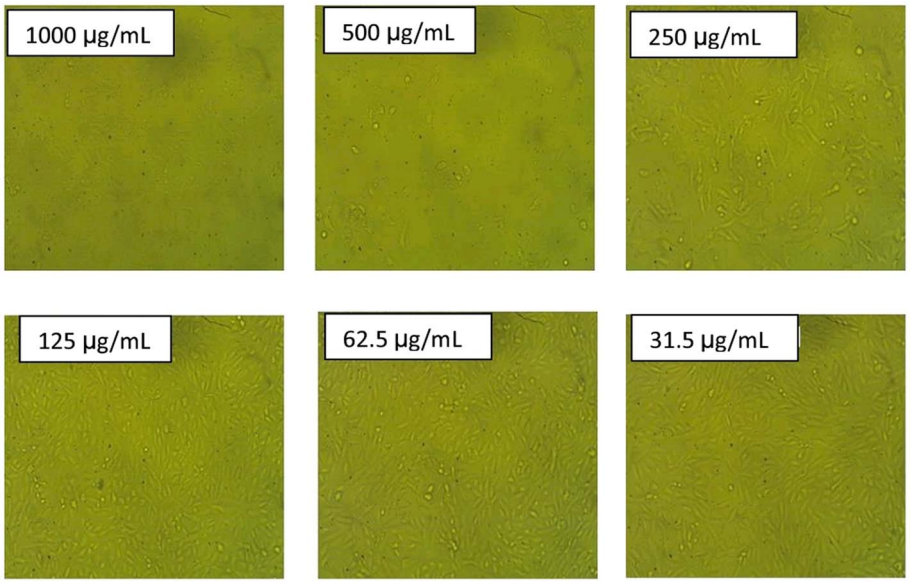

Fig. 10 Morphological effect of GT-NZVAl (40) on WI-38 cells at different concentrations. The data for the scale bar are discussed in the ESI (SI.1).†

silver nanoparticles of various sizes, and found that gold nanoparticles with smaller sizes exhibit anti-inflammatory impacts by diminishing the production of pro-inflammatory cytokines in immune cells. Kim *et al.*[49] investigated the cellular uptake of magnetic nanoparticles and their effects on inflammatory responses in lung epithelial cells, and suggested that magnetic nanoparticles can constrain the production of pro-inflammatory cytokines, indicating their potential anti-inflammatory activity. Bi *et al.*[50] discussed the toxic effects of microscale metal oxides, including zero-valent metallic compounds, on immune cells, and highlighted that these compounds can induce inflammation and immune responses, suggesting their potential modulatory effects on inflammatory processes.

Black tea has been recognized for its potential antimicrobial activity against a variety of microorganisms. The antimicrobial effects of black tea can be attributed to its polyphenols, particularly catechins, and theaflavins, which have been shown to reveal inhibitory impacts against bacteria, viruses, and fungi. Here are a few previous studies that provide information on the antimicrobial activity of black tea. Barroso *et al.*[51] investigated the antimicrobial activity of green and black tea extracts against

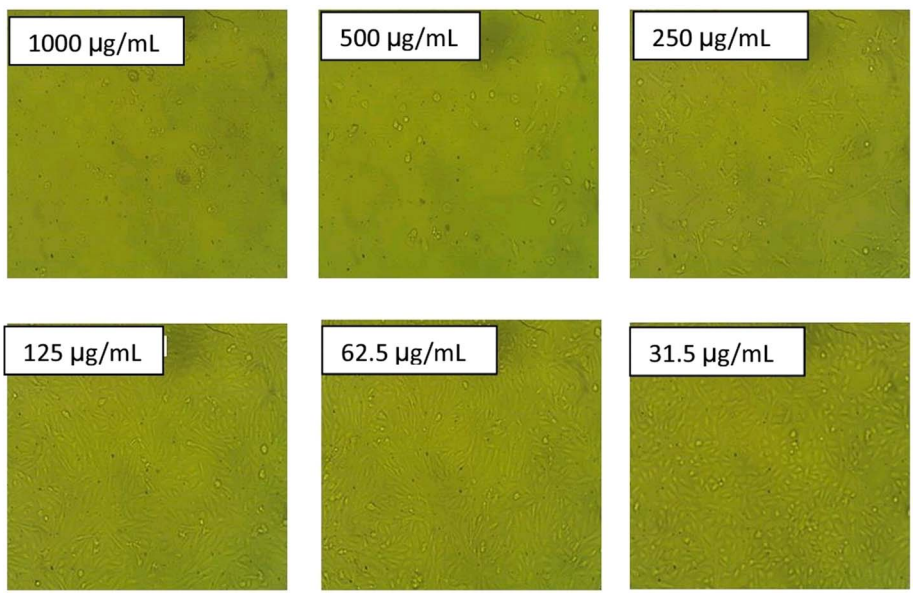

Fig. 11 Effect of GT-NZVAl (100) on WI-38 cells at different concentrations. The data for the scale bar are discussed in the ESI (SI.2).†

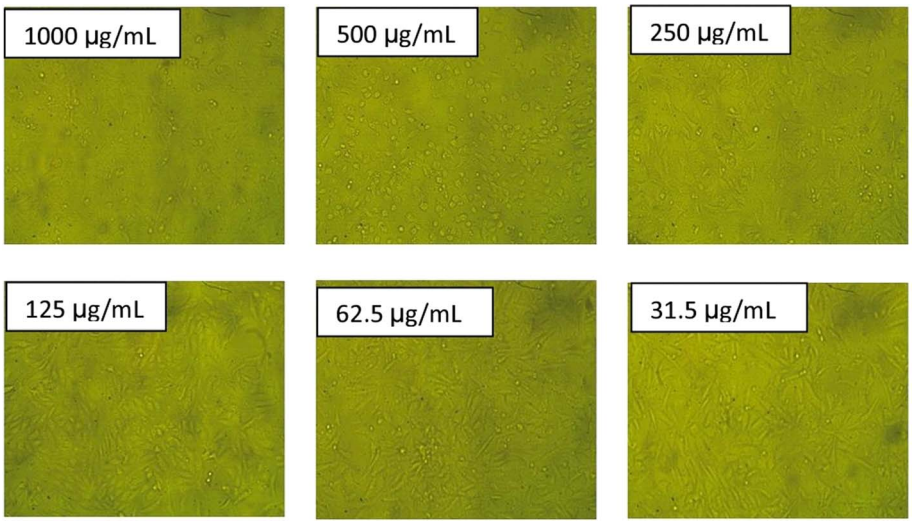

Fig. 12 Effect of doxorubicin on WI-38 cells at different concentrations. The data for the scale bar are discussed in the ESI (SI.3).†

cariogenic bacteria implicated in dental caries, and found that both green and black tea extracts possess significant inhibitory effects against these bacteria. Friedman *et al.*[52] evaluated the bactericidal activities of various essential oils and their components against several foodborne pathogens, including *Salmonella enterica*. They showed that black tea extract exhibited antimicrobial effects against *S. enterica*, indicating its potential as a natural antimicrobial agent. Mandalari *et al.*[53] investigated the antimicrobial activity of flavonoids extracted from bergamot peel, which is a component of Earl Grey black tea, and found that the flavonoids demonstrated antimicrobial effects against several bacteria, including *Staphylococcus aureus* and *Escherichia coli*.

Williamson *et al.*[54] provided an overview of intervention studies investigating the bioavailability and bioefficacy of polyphenols, including those found in tea. They discussed the potential antimicrobial effects of tea polyphenols and their impact on human health. Zero-valent aluminum, also known as elemental aluminum (Al^0), is primarily known for its chemical reactivity rather than its anti-inflammatory activity. Aluminum, in its elemental form, is highly reactive and readily oxidizes in the presence of oxygen and water. It develops a thin layer of aluminum oxide (Al_2O_3) on its surface, serving as a protective barrier against additional oxidation. While aluminum has been broadly probed for its potential toxicity and adverse health effects, such as its association with neurodegenerative disorders, research on its anti-inflammatory properties is limited. Aluminum is often implicated in promoting inflammation and immune responses when it enters the body as certain aluminum compounds, such as aluminum salts used in vaccines or aluminum-containing antacids.

Zero-valent metallic compounds, including zero-valent metals and their nanoparticles, have been investigated for their antimicrobial activity against various microorganisms. Here are some references that discuss the antimicrobial properties of zero-valent metallic compounds. Choi *et al.*[55] focused on silver (Ag) nanoparticles, a common zero-valent metallic compound, and their antimicrobial effects, and found that silver nanoparticles display potent antimicrobial effectiveness against a wide range of microorganisms, including both bacteria and fungi. Guzman *et al.*[56] investigated the synthesis and antibacterial activity of silver nanoparticles, and showed that silver nanoparticles possess potent antimicrobial effects against both Gram-positive and Gram-negative bacteria, signifying their potential utility as antimicrobial agents. Seil *et al.*[57] provided an overview of the antimicrobial applications of

Table 1 Free radical scavenging activity of GT-NZVAl compared with Trolox. Mean ± SE were statistically validated with three replicates ($n = 3$)[a]

Conc. μg mL^{-1}	DPPH scavenging % of Trolox	DPPH scavenging % of GT-NZVAl (40)	DPPH scavenging % of GT-NZVAl (100)
100	92.2 ± 0.01^{b}	93.6 ± 0.05^{ab}	97.6 ± 0.05^{b}
50	86.5 ± 0.01^{b}	88.3 ± 0.03^{ab}	93.5 ± 0.03^{b}
25	83.3 ± 0.01^{b}	84.1 ± 0.02^{ab}	92.2 ± 0.02^{b}
12.5	72.4 ± 0.03^{b}	76.4 ± 0.01^{ab}	85.2 ± 0.01^{b}
6.25	65.6 ± 0.01^{b}	70.4 ± 0.01^{ab}	79.6 ± 0.01^{b}
3.12	54.2 ± 0.02^{b}	61.1 ± 0.01^{ab}	67.2 ± 0.01^{b}
1.56	41.4 ± 0.01^{b}	$50.4^{a} \pm 0.01^{ab}$	$57.6^{a} \pm 0.01^{b}$

[a] Statistical analysis was conducted using one-way ANOVA, followed by Duncan's multiple comparison tests, with significance set at $P < 0.05$.

Table 2 Effect of standard indomethacin and GT-NZVAl on hemolysis inhibition %[a]

Conc. μg ml^{-1}	Haemolysis inhibition % standard (Indo.)	Haemolysis GT-NZVAl (40)	Haemolysis GT-NZVAl (100)
1000	94.2 ± 0.01	95.3 ± 0.01	98.3 ± 0.01
800	90.5 ± 0.02	91.6 ± 0.03	94.6 ± 0.03
600	82.2 ± 0.01	88.2 ± 0.02	90.2 ± 0.02
400	73.1 ± 0.02	81.3 ± 0.01	88.3 ± 0.01
200	60.3 ± 0.01	65.4 ± 0.05	76.4 ± 0.05
100	51.3 ± 0.01	57.1 ± 0.03	65.1 ± 0.03

[a] Statistical analysis was carried out by one-way ANOVA followed by Duncan's multiple comparison tests. Significance was set at $P < 0.05$.

Table 3 IC_{50} values of COX-1 and COX-2 and selectivity index (SI) values for comparing the *in vitro* anti-inflammatory activities of GT-NZVAl and the celecoxib standard[a]

Drug	IC50 (COX-1) (μM)	IC50 (COX-2) (μM)	Selectivity index (SI)
Celecoxib	0.50 ± 0.15[a]	0.09 ± 0.001[a]	5.56[a]
GT-NZVAl (40)	2.60 ± 0.08[c]	1.25 ± 0.01[c]	2.08[c]
GT-NZVAl (100)	1.40 ± 0.07[b]	0.16 ± 0.01[b]	8.75[b]

[a] Statistical analysis was conducted using one-way ANOVA, followed by Duncan's multiple comparison tests, with significance set at $P < 0.05$.

nanotechnology, including zero-valent metallic compounds. They discusses the antimicrobial properties of various metallic nanoparticles, such as silver, copper, and zinc, and their potential mechanisms of action.

Ruparelia *et al.*[58] compared the antimicrobial activity of silver and copper nanoparticles against different strains of bacteria, and highlighted the strain-specific nature of the antimicrobial effects of these metallic nanoparticles. Zero-valent metallic compounds, such as zero-valent metals and their nanoparticles, have been studied for their potential antioxidant activity. Here is a discussion of a few previous reports that discuss the antioxidant properties of zero-valent metallic compounds. Huang *et al.*[59] examined the impact of superparamagnetic iron oxide nanoparticles (SPIONs) on the proliferation of human mesenchymal stem cells (hMSCs), and suggested that SPIONs possess antioxidant properties and can enhance the antioxidant capacity of hMSCs. Díez *et al.*[60] focused on the antioxidant and pro-oxidant properties of nickel compounds, including zero-valent nickel, and discussed the potential antioxidant effects of zero-valent nickel and its influence on oxidative stress.

Díaz-Visurraga *et al.*[42] studied the antioxidant activity of copper nanoparticles synthesized using a polyol method, and demonstrated that copper nanoparticles display antioxidant effects, as verified by their capability to scavenge free radicals and inhibit lipid peroxidation. Zhou *et al.*[61] investigated zinc oxide nanowires' biodegradability and biocompatibility, and suggested that ZnO nanowires possess antioxidant properties and can scavenge reactive oxygen species (ROS).

The relationship between the surface area, pore size, and biological activity, such as antioxidant or antimicrobial efficacy, is influenced by several factors. A higher surface area typically enhances biological activity due to the increased exposure and interaction sites for reactive molecules or microorganisms. A larger surface area allows more reactive oxygen species (ROS) to interact with antioxidant molecules, improving scavenging

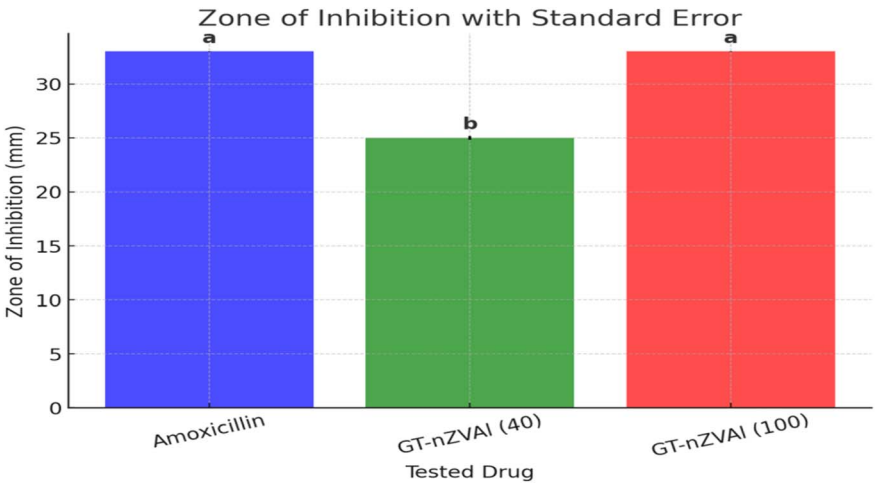

Fig. 13 Inhibition width zones (in mm). The values are described as mean ± SE, with superscript significance letters (a, b, and c) placed above each column. This indicates significance between groups at $P \leq 0.05$.

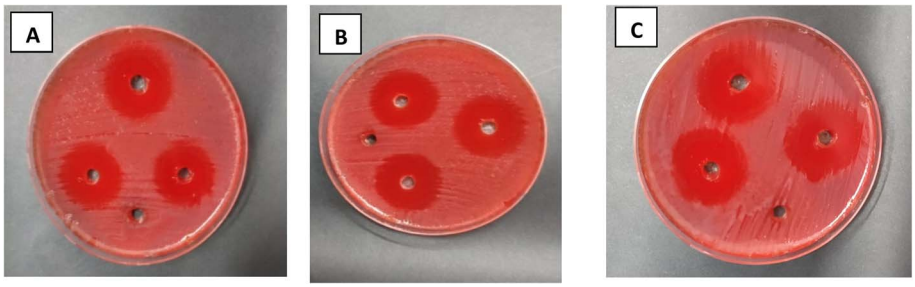

Fig. 14 Inhibition zone macroscopical images. Inhibition width zones for (A) GT-NZVAl (40), (B) GT-NZVAl (100) and (C) amoxicillin.

efficiency.[62,63] A greater surface area increases the contact points for antimicrobial agents with microbial cell membranes, thereby enhancing efficacy.[64,65] The pore size plays a crucial role in determining the accessibility and efficiency of biological activity; whereby small pores enhance the adsorption of smaller molecules, such as free radicals, boosting antioxidant activity.[66] Also, selective antimicrobial action is promoted by allowing smaller molecules to penetrate cells while excluding larger pathogens.[67] In addition, materials with an optimized surface area and pore size can effectively interact with ROS, enhancing the adsorption of radicals.[68] Furthermore, porous structures with nanoscale pores can directly disrupt microbial membranes through physical interactions. Furthermore, these materials can serve as carriers for antimicrobial agents, facilitating prolonged release and enhanced activity.[63,65]

Green tea (*Camellia sinensis*) has been effectively utilized in the green synthesis of zero-valent metal nanoparticles, notably zero-valent iron (ZVI), enhancing their biological activities. The polyphenols and antioxidants present in green tea serve as natural reducing and stabilizing agents, promoting the synthesis of nanoparticles without the necessity for toxic chemicals. For instance, a study demonstrated the successful synthesis of ZVI using green tea extract, where the extract not only reduced iron ions but also stabilized the nanoparticles, resulting in improved reactivity and environmental remediation capabilities. The synthesized ZVI exhibited significant efficiency in removing contaminants, such as chromium(VI), from aqueous solutions, highlighting its potential in environmental applications.[69] In addition to environmental remediation, green tea-mediated nanoparticles have shown promising biological activities. The inherent antimicrobial properties of green tea, attributed to its rich polyphenol content, are enhanced when combined with metal nanoparticles. Research indicates that green tea-synthesized iron nanoparticles demonstrate considerable antibacterial efficacy against diverse pathogens, including *E. coli* and *S. aureus*. The mechanism involves the generation of reactive oxygen species (ROS) and the disruption of microbial cell membranes, leading to cell death.[70]

Furthermore, the antioxidant properties of green tea are well-documented, primarily due to compounds like epigallocatechin-3-gallate (EGCG), which detoxify free radicals and diminish oxidative stress. These antioxidant properties can

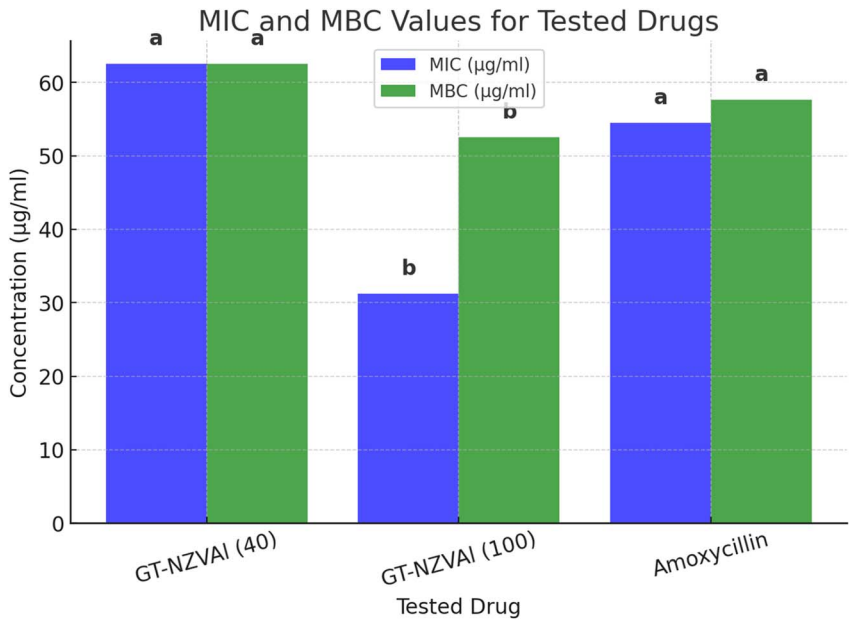

Fig. 15 The bar chart for MIC and MBC values of the tested drugs, with superscript significance letters above each column.

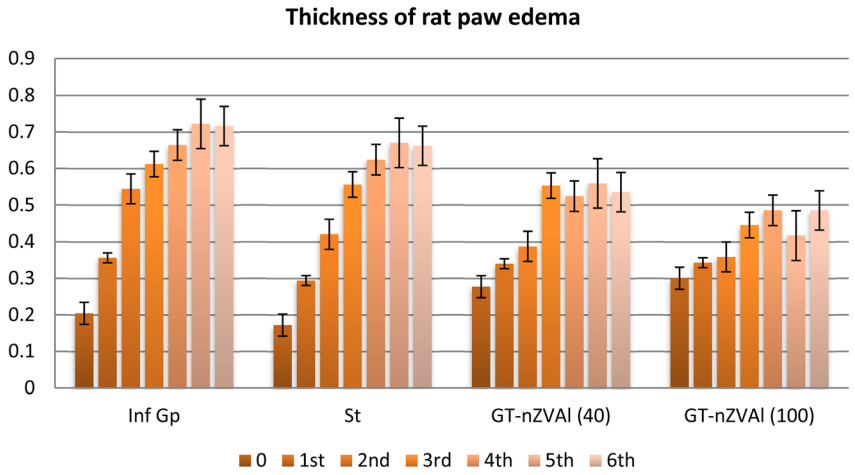

Fig. 16 Thickness of rat paw edema. The values are described as the mean ± SE ($n = 7$ rats per group) at $P \leq 0.05$.

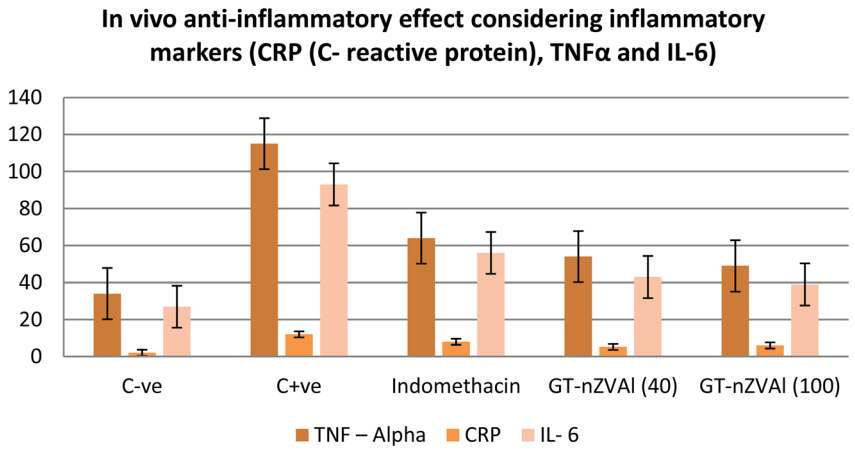

Fig. 17 *In vivo* anti-inflammatory effect considering the inflammatory markers (CRP (C-reactive protein), TNFα and IL-6). The values are described as the mean ± SE ($n = 7$ rats per group) at $P \leq 0.05$.

be imparted to nanoparticles during synthesis, potentially augmenting their therapeutic efficacy. For example, green tea-synthesized silver nanoparticles have demonstrated enhanced antioxidant activity, which could be valuable in mitigating oxidative stress-related cellular damage.[11]

Additionally, green tea possesses anti-inflammatory properties, which are advantageous in decreasing inflammation-related health matters. The active compounds in green tea, such as catechins, have been shown to suppress the synthesis of pro-inflammatory cytokines, thereby reducing inflammation. Incorporating these properties into nanoparticle synthesis could lead to novel therapeutic agents with combined antimicrobial, antioxidant, and anti-inflammatory effects.

5. Conclusion

Nano zero-valent aluminum (NZVAl) exhibits exceptional reactivity and reduction capabilities; hence, this study synthesized it by a green synthesis method (GT-NZVAl), which offers numerous advantages, including the production of carbon and oxide outer layers that enhance its stability, cost-effectiveness, and safety. XRD, BET, TEM, and SEM were employed to describe the green-synthesized nano zero-valent aluminum fabricated at concentrations of 40 and 100 g L^{-1}. Subsequently, the GT-NZVAl (40 and 100) were examined to assess their antioxidant activity utilizing the DPPH radical scavenging method. Also, HPLC analysis, and *in vitro* antioxidant activity (DPPH assay), anti-inflammatory activity (membrane stabilization *via* COX-1 and COX-2), antimicrobial efficacy (minimum inhibitory concentration and minimum bactericidal concentration), and *in vivo* anti-inflammatory activity (C-reactive protein, tumor necrosis factor-alpha, interleukin-6 assays) tests were performed. GT-nZVAl (100) demonstrated antioxidant activity comparable to that of GT-nZVAl (40) and the standard ascorbic acid. The antioxidant efficacy increased in a dose-dependent manner across all administered doses. GT-NZVAl exhibited anti-inflammatory efficacy comparable to that of indomethacin. The dose-dependent anti-inflammatory activity of GT-NZVAl at two doses against COX-1 and COX-2 was augmented. *In vivo* anti-inflammatory investigations indicated that the novel

nanoparticle formulation could diminish inflammation. The MTT experiment revealed that GT-NZVAl (40) and (100) exhibited cytotoxicity against the normal human diploid cell line WI-38, with IC_{50} values of 302.96 and 382.99 μg ml^{-1}, respectively.

Data availability

All the authors confirm that the data supporting the findings of this study are available within the article and its ESI† (the data are confidential).

Conflicts of interest

There are no conflict to declare.

References

1 S. Hasan, *Res. J. Recent Sci.*, 2015, **2277**, 2502.
2 M. Hassellöv, J. W. Readman, J. F. Ranville and K. Tiede, *Ecotoxicology*, 2008, **17**, 344–361.
3 A. S. Mahmoud, R. S. Farag, M. M. Elshfai, L. A. Mohamed and S. M. Ragheb, *Air, Soil Water Res.*, 2019, **12**, 1178622119878707.
4 C. Wu, L. Hus, P. Chiang, J. Liu, W. Kuan, C. Chen, Y. Tzou, M. Wang and C. Hwang, *Water Res.*, 2013, **47**, 2583–2591.
5 P. Nidheesh, J. Khatri, T. A. Singh, R. Gandhimathi and S. Ramesh, *Chemosphere*, 2018, **200**, 621–631.
6 T. Shahwan, S. A. Sirriah, M. Nairat, E. Boyacı, A. E. Eroğlu, T. B. Scott and K. R. Hallam, *Chem. Eng. J.*, 2011, **172**, 258–266.
7 A. Karam, K. Zaher and A. S. Mahmoud, *Air, Soil Water Res.*, 2020, **13**, 1178622120908273.
8 C. P. Devatha and A. K. Thalla, in *Synthesis of Inorganic Nanomaterials*, Elsevier, 2018, pp. 169–184.
9 X. Han, Y. Zhao, F. Zhao, F. Wang, G. Tian and J. Liang, *Colloids Surf., A*, 2023, **656**, 130412.
10 T. Wang, J. Lin, Z. Chen, M. Megharaj and R. Naidu, *J. Cleaner Prod.*, 2014, **83**, 413–419.
11 J. Flieger, W. Franus, R. Panek, M. Szymańska-Chargot, W. Flieger, M. Flieger and P. Kołodziej, *Molecules*, 2021, **26**, 4986.
12 S. Machado, S. Pinto, J. Grosso, H. Nouws, J. T. Albergaria and C. Delerue-Matos, *Sci. Total Environ.*, 2013, **445**, 1–8.
13 C. Cabrera, R. Artacho and R. Giménez, *J. Am. Coll. Nutr.*, 2006, **25**, 79–99.
14 D. L. McKay and J. B. Blumberg, *J. Am. Coll. Nutr.*, 2002, **21**, 1–13.
15 U. J. Unachukwu, S. Ahmed, A. Kavalier, J. T. Lyles and E. J. Kennelly, *J. Food Sci.*, 2010, **75**, C541–C548.
16 D. Grassi, G. Desideri, G. Croce, S. Tiberti, A. Aggio and C. Ferri, *Curr. Pharm. Des.*, 2009, **15**, 1072–1084.
17 A. S. Mahmoud, R. S. Farag and M. M. Elshfai, *Egypt. J. Pet.*, 2020, **29**, 9–20.
18 R. Hao, D. Li, J. Zhang and T. Jiao, *Nanomaterials*, 2021, **11**, 650.
19 T. Mareedu, V. Poiba and M. Vangalapati, *Mater. Today: Proc.*, 2021, **42**, 1498–1501.
20 R. S. Farag, M. M. Elshfai, A. S. Mahmoud, M. K. Mostafa and R. W. Peters, *Environ. Div.*, 2018, 307–317.
21 O. A. Fouad, S. M. Saleh, N. Nasser, G. G. Mohamed, M. A. Omar and M. R. Mostafa, *Microchem. J.*, 2025, **211**, 113088.
22 S. Bhakya, S. Muthukrishnan, M. Sukumaran and M. Muthukumar, *Appl. Nanosci.*, 2016, **6**, 755–766.
23 C. A. Anosike, O. Obidoa and L. U. Ezeanyika, *Daru, J. Pharm. Sci.*, 2012, **20**, 1–7.
24 R. J. Kulmacz and W. E. Lands, *Prostaglandins*, 1983, **25**, 531–540.
25 P. Wayne, *Performance Standards for Antimicrobial Susceptibility Testing*, CLSI document M100-S17, 2005.
26 I. Castillo-Juárez, F. Rivero-Cruz, H. Celis and I. Romero, *J. Ethnopharmacol.*, 2007, **114**, 72–77.
27 G. French, *J. Antimicrob. Chemother.*, 2006, **58**, 1107–1117.
28 R. Domenjoz, W. Theobald, S. EG and K. Morsdorf, *Arch. Int. Pharmacodyn. Ther.*, 1955, **103**, 341–352.
29 E. L. Kilpatrick and D. M. Bunk, *Anal. Chem.*, 2009, **81**, 8610–8616.
30 J. T. Afshari, N. Ghomian, A. Shameli, M. Shakeri, M. Fahmidehkar, E. Mahajer, R. Khoshnavaz and M. Emadzadeh, *BMC Pregnancy Childbirth*, 2005, **5**, 1–5.
31 W. Łuczaj and E. Skrzydlewska, *Prev. Med.*, 2005, **40**, 910–918.
32 K. Gottimukkala, R. Harika, D. Zamare and J. N. Biother, *Discov*, 2017, **7**, 151.
33 C. Xiao, H. Li, Y. Zhao, X. Zhang and X. Wang, *J. Environ. Manage.*, 2020, **275**, 111262.
34 F. Zhu, S. Ma, T. Liu and X. Deng, *J. Cleaner Prod.*, 2018, **174**, 184–190.
35 M. Fazlzadeh, K. Rahmani, A. Zarei, H. Abdoallahzadeh, F. Nasiri and R. Khosravi, *Adv. Powder Technol.*, 2017, **28**, 122–130.
36 S. Liu, S. Yang, X. Bao, Y. Li, M. Wang and D. Zhao, *J. Cleaner Prod.*, 2022, **366**, 133013.
37 N. Tan, Z. Yang, X.-b. Gong, Z.-r. Wang, T. Fu and Y. Liu, *Sci. Total Environ.*, 2019, **650**, 2567–2576.
38 J. Yang, S. Wang, N. Xu, Z. Ye, H. Yang and X. Huangfu, *J. Hazard. Mater.*, 2021, **419**, 126461.
39 A. H. Sadek and M. K. Mostafa, *Appl. Water Sci.*, 2023, **13**, 34.
40 M. Ahmed, M. M. El-Shafei, A. S. Mahmoud, M. Mostafa, A. Karam and R. Peters, Study the degradation and adsorption processes of organic matters from domestic wastewater using chemically prepared and green synthesized nano zero-valent Iron, in *2019 AIChE Annual Meeting*, AIChE, 2019.
41 L. Huang, X. Weng, Z. Chen, M. Megharaj and R. Naidu, *Spectrochim. Acta, Part A*, 2014, **130**, 295–301.
42 A. Shawn M, M. Senso and D. L. Golem, *J. Int. Soc. Sports Nutr.*, 2010, **7**(1), 11.
43 C.-N. Zhao, G.-Y. Tang, S. Yu Cao, X. Yu Xu, R. You Gan, Q. Liu, Q. Qian Mao, A. Shang and H. Bin Li, *Antioxidants*, 2019, **8**, 215.
44 S. Kuriyama, T. Shimazu, K. Ohmori, N. Kikuchi, N. Nakaya, Y. Nishino, Y. Tsubono and I. Tsuji, *Jama*, 2006, **296**, 1255–1265.

45 X. Meng, Y. Li, S. Li, R. Y. Gan and H. B. Li, *Compr. Rev. Food Sci. Food Saf.*, 2018, **17**, 472–495.
46 W. C. Reygaert, *Int. J. Mol. Sci.*, 2017, **3**, 1.
47 C.-L. Shen, V. von Bergen, M.-C. Chyu, M. R. Jenkins, H. Mo, C.-H. Chen and I.-S. Kwun, *Nutr. Res.*, 2012, **32**, 897–910.
48 H. J. Yen, S. h. Hsu and C. L. Tsai, *Small*, 2009, **5**, 1553–1561.
49 J.-S. Kim, T.-J. Yoon, K.-N. Yu, M. S. Noh, M. Woo, B.-G. Kim, K.-H. Lee, B.-H. Sohn, S.-B. Park and J.-K. Lee, *J. Vet. Sci.*, 2006, **7**, 321–326.
50 J. Bi, C. Mo, S. Li, M. Huang, Y. Lin, P. Yuan, Z. Liu, B. Jia and S. Xu, *Biomater. Sci.*, 2023, **11**, 4151–4183.
51 H. Barroso, R. Ramalhete, A. Domingues and S. Maci, *J. Oral Microbiol.*, 2018, **10**, 1481322.
52 M. Friedman, P. R. Henika and R. E. Mandrell, *J. Food Prot.*, 2002, **65**, 1545–1560.
53 G. Mandalari, R. N. Bennett, G. Bisignano, A. Saija, G. Dugo, R. B. Lo Curto, C. B. Faulds and K. W. Waldron, *J. Agric. Food Chem.*, 2006, **54**, 197–203.
54 G. Williamson and C. Manach, *Am. J. Clin. Nutr.*, 2005, **81**, 243S–255S.
55 O. Choi, K. K. Deng, N. Jung Kim, L. Ross Jr, R. Y. Surampalli and Z. Hu, *Water Res.*, 2008, **42**, 3066–3074.
56 M. Guzman, J. Dille and S. Godet, *Nanomedicine*, 2012, **8**, 37–45.
57 J. T. Seil and T. J. Webster, *Int. J. Nanomed.*, 2012, 2767–2781.
58 J. P. Ruparelia, A. K. Chatterjee, S. P. Duttagupta and S. Mukherji, *Acta Biomater.*, 2008, **4**, 707–716.
59 D.-M. Huang, J.-K. Hsiao, Y.-C. Chen, L.-Y. Chien, M. Yao, Y.-K. Chen, B.-S. Ko, S.-C. Hsu, L.-A. Tai and H.-Y. Cheng, *Biomaterials*, 2009, **30**, 3645–3651.
60 A. M. Díez, V. C. Fernandes, M. M. Moreira, M. Pazos, M. A. Sanromán, T. Albergaria and C. D. Matos, *Process Saf. Environ. Prot.*, 2023, **176**, 1089–1100.
61 J. Zhou, N. S. Xu and Z. L. Wang, *Adv. Mater.*, 2006, **18**, 2432–2435.
62 A. Menichetti, A. Mavridi-Printezi, D. Mordini and M. Montalti, *J. Funct. Biomater.*, 2023, **14**, 244.
63 L. Wang, C. Hu and L. Shao, *Int. J. Nanomed.*, 2017, 1227–1249.
64 A. K. Alzubaidi, W. J. Al-Kaabi, A. A. Ali, S. Albukhaty, H. Al-Karagoly, G. M. Sulaiman, M. Asiri and Y. Khane, *Appl. Sci.*, 2023, **13**, 2182.
65 M. Abbasi, R. Gholizadeh, S. R. Kasaee, A. Vaez, S. Chelliapan, F. Fadhil Al-Qaim, I. F. Deyab, M. Shafiee, Z. Zareshahrabadi and A. M. Amani, *Sci. Rep.*, 2023, **13**, 5987.
66 L. Gabrielyan, H. Badalyan, V. Gevorgyan and A. Trchounian, *Sci. Rep.*, 2020, **10**, 13145.
67 M. T. Shaaban, B. S. Mohamed, M. Zayed and S. M. El-Sabbagh, *BMC Biotechnol.*, 2024, **24**, 8.
68 R. F. Hamarawf, *RSC Adv.*, 2024, **14**, 9080–9098.
69 D. R. Eddy, D. Nursyamsiah, M. D. Permana, Solihudin, A. R. Noviyanti and I. Rahayu, *Materials*, 2022, **15**, 332.
70 S. Borehalli Mayegowda, A. Roy, M. NG, S. Pandit, S. Alghamdi, M. Almehmadi, M. Allahyani, N. S. Awwad and R. Sharma, *Front. Cell. Infect. Microbiol.*, 2023, **13**, 1224778.